

Strong coupling between a single NV spin and the torsional mode of diamonds levitating in an ion trap

T. Delord¹, L. Nicolas¹, Y. Chassagneux¹, and G. Hétet¹

¹*Laboratoire Pierre Aigrain, Ecole normale supérieure,
PSL Research University, CNRS, Université Pierre et Marie Curie,
Sorbonne Universités, Université Paris Diderot, Sorbonne Paris-Cité,
24 rue Lhomond, 75231 Paris Cedex 05, France.*

A scheme for strong coupling between a single atomic spin and the torsional mode of levitating nanoparticles is proposed. The idea is based on spin read-out of NV centers embedded in aspherical nanodiamonds levitating in an ion trap. We show that the torsional mode of nanodiamonds can be strongly coupled to the electronic spin of the NV center using a homogeneous transverse magnetic field. Further, we demonstrate that cooling to the torsional ground state can be performed efficiently using a combination of microwaves and weak optical pulses at room temperature.

Experiments in the field of opto-mechanics showed control of macroscopic mechanical oscillators very close to their ground state of motion [1]. These accomplishments provide great opportunities to observe quantum superpositions with macroscopic systems. Although progress are being made with room temperature oscillators [2–4], the difficulty in most experiments is that they require cooling of the oscillators down to milliKelvin temperatures because they are clamped to a structure. Inspired by ideas for mechanical control of oscillating cantilevers using magnetic field sensitive probes [5–8], trapped macroscopic objects coupled to single spins via magnetic field gradients are envisioned [9]. There, the mechanical support is completely removed so one could operate at room temperature and reach high quality factors [10]. Further, the spins coupled to the massive object can be used to create matter wave interference [11] and Schrödinger cat states where the spin is entangled with the collective oscillator motion [9, 12].

Many experimental protocols are being explored to couple the center of mass mode of levitating objects to single spins, most of which use diamonds with embedded Nitrogen Vacancy (NV) centers in dipole traps [9]. In recent experiments however, despite the mechanical support being completely removed, light scattering from the optically levitated object significantly alters the photophysical properties of the NV centers [13–15]. Although advances have been made in this direction [16], many groups indeed observe strong heating at low vacuum pressures which quenches the NV photoluminescence [13, 17, 18]. Further, strong coupling between a single spin and the center of mass mode requires very high magnetic field gradients in the range of 10^5 to 10^7 T/m [6, 12], which is experimentally challenging.

In this paper, we present a scheme for strong coupling of a single spin to levitating nanoparticles that leverages both issues. First, we propose using a Paul trap for torsional confinement of charged aspherical nanodiamonds. Second, we propose to couple the torsional degree of freedom to the spin of embedded NV centers using homogeneous magnetic fields. The proposal makes use of the inherent quantization axis of the NV center together with

the possibility to perform room temperature read-out of its electronic spin. We show that homogeneous magnetic fields in the range of tens of milliteslas together with prolate nanodiamonds is enough to reach strong coupling and efficient ground state cooling of the torsional mode.

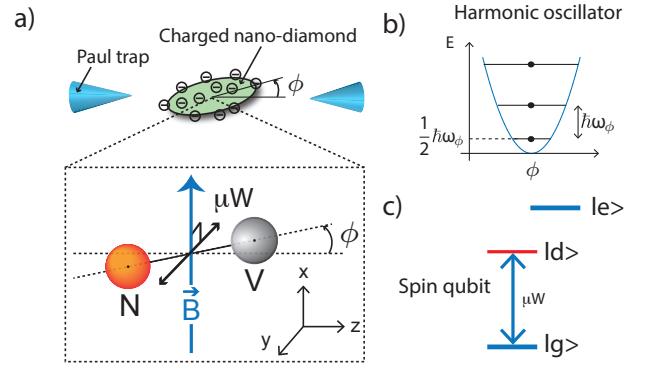


FIG. 1: a) Schematics showing a prolate nanodiamond levitating in a needle Paul trap. The spin of a nitrogen vacancy center inside the diamond senses the rotation of the particle in the presence of a transverse B-field. b) Harmonic potential energy as a function of the angle ϕ between the particle and the main trap axis, with torsional frequency ω_ϕ . c) NV center level scheme in the basis dressed by the transverse magnetic field.

Fig. 1-a) shows a schematics of a prolate diamond levitating in a needle Paul trap. The coupling between the torsional mode and the NV center relies on the microwave driving of the electronic spin of an NV center inside this aspherical particle. The NV centers in diamond consist of a substitutional nitrogen atom (N) associated with a vacancy (V) in an adjacent lattice site of the diamond matrix. This defect behaves as an artificial atom trapped in the diamond matrix and exhibits a strong photoluminescence in the red which allows the detection of individual NV defects using optical confocal microscopy at room temperature. It is also possible to optically initialize and read-out the electronic spin of the NV center thanks to the presence of a metastable level and an intersystem crossing [19]. Compared to single atoms where the quan-

tization axis is defined with respect to the B-field, with NV centers, the spin-spin interaction sets a preferential direction along the NV axis, as shown in the inset.

In [6], the oscillations of a cantilever produce a time-varying magnetic field that causes Zeeman shifts of the electronic spin. This shift can be measured within a fraction of a millisecond by detecting the electronic spin state. The coupling constant can exceed both the electronic spin coherence time of NV centers in the bulk and the damping rate of high-Q mechanical resonators, so that the spin becomes strongly coupled to center of mass motion. Here instead, one considers a nanodiamond levitating in a Paul trap with a single NV center in a homogeneous magnetic field. We show that similar coupling conditions can be reached and that using the torsional mode enables reaching oscillation frequencies that are higher than the center of mass mode for the same surface charge density.

I. TORSIONAL CONFINEMENT IN A PAUL TRAP

NV centers were already detected with diamonds levitating in a Paul trap [20, 21]. In [21], the electronic spin resonance of nanodiamonds was employed to demonstrate their angular stability. The torsional confinement was interpreted using a model that involves one rotational axis. Here, we treat the more general case of a symmetric rotor : we use classical mechanics to show that its rotation about the two axes is ruled by a Mathieu equation and derive the corresponding effective torsional frequency. For this, let us consider the following quadratic static electric potential: $V_E = \frac{V}{z_0^2} (z^2 - \frac{1}{2}x^2 - \frac{1}{2}y^2)$, where $V = V_{dc} + V_{ac} \cos(\Omega t)$ is the voltage applied on the needle electrode, oscillating at a frequency $\Omega/2\pi$.

We take a particle with total surface charge Q , and assume that the charge centroid coincides with the center of mass at all times. We then integrate the torque applied on each surface element over the whole surface of the particle. To calculate the torque applied by the electric field on the particle, we introduce a rotating frame XYZ whose axes are fixed to the particle and parallel to its principal axes of inertia. We consider the particle to be symmetric about its Z axis and hence use only two Euler angle ϕ_1, ϕ_2 to define the XYZ frame : ϕ_1 for a first rotation of the initial frame xyz about the y axis and ϕ_2 for a second rotation of the rotated frame $x'y'z'$ about the rotated x' axis. The matrix allowing one to obtain XYZ from xyz is :

$$R(\phi_1, \phi_2) = \begin{pmatrix} \cos \phi_1 & 0 & \sin \phi_1 \\ 0 & 1 & 0 \\ -\sin \phi_1 & 0 & \cos \phi_1 \end{pmatrix} \begin{pmatrix} 1 & 0 & 0 \\ 0 & \cos \phi_2 & -\sin \phi_2 \\ 0 & \sin \phi_2 & \cos \phi_2 \end{pmatrix}. \quad (1)$$

One can then calculate the torque applied by the electric field to the particle. For an element of surface dS

with charge dQ in the xyz frame we have :

$$d\vec{M} = \frac{dQV}{z_0^2} \begin{pmatrix} -3yx \\ 3xz \\ 0 \end{pmatrix}. \quad (2)$$

After changing the basis to the rotating frame XYZ and integrating over the whole surface of the particle, one obtains :

$$\begin{aligned} M_X &= 3 \frac{V}{z_0^2} \cos^2 \phi_1 \iint (Z^2 - Y^2) dQ \frac{\sin(2\phi_2)}{2} \\ &\quad \text{and} \\ M_Y &= 3 \frac{V}{z_0^2} \cos \phi_2 \iint (Z^2 - X^2) dQ \frac{\sin(2\phi_1)}{2}. \end{aligned} \quad (3)$$

Given the symmetry of the particle no torque is applied along the Z axis, we consider the particle not to rotate about this axis. If one consider small angles $\phi_1, \phi_2 \ll 1$ and neglect second order terms, the Euler equation for the angles then becomes :

$$\begin{aligned} \ddot{\phi}_1 &= 3 \frac{V}{I_y z_0^2} \iint (Z^2 - X^2) dQ \phi_1 \\ \ddot{\phi}_2 &= 3 \frac{V}{I_x z_0^2} \iint (Z^2 - Y^2) dQ \phi_2. \end{aligned} \quad (4)$$

These are Mathieu equations for the angles ϕ_1, ϕ_2 and within their stability conditions they yield a harmonic confinement for both rotation angles of the particle, at secular frequencies :

$$\omega_\mu = \frac{\Omega}{2} \sqrt{a_\mu + \frac{q_\mu^2}{2}}, \quad (5)$$

with dimensionless parameters :

$$\begin{aligned} q_\mu &= 3 \frac{QS_\mu}{I_\mu} \frac{V_{ac}}{z_0^2} \frac{1}{\Omega^2}, \\ a_\mu &= -6 \frac{QS_\mu}{I_\mu} \frac{V_{dc}}{z_0^2} \frac{1}{\Omega^2}, \end{aligned} \quad (6)$$

where $\mu = X, Y$, $S_X = R_Z^2 - R_Y^2$, $S_Y = R_Z^2 - R_X^2$ with $R_\mu^2 = \iint \mu^2 dQ/Q$. At this stage, the calculations do not assume a homogeneous charge distribution.

The torsional confinement not only depends on the charge to mass ratio and on the generated potential, like for the center of mass, but also crucially on the geometry of the particle. The factor QS_μ/I_μ in eq. (6), which one might rewrite $\iint (Z^2 - X^2) dQ / (\iiint Y^2 dm)$ for $\mu = Y$, can indeed be increased using an asymmetric particle. This will be further discussed in section III A.

II. TORSIONAL COOLING

Fig. 1-b) shows the harmonic potential for a small angle ϕ obtained from equation (5). Just like for the center of mass mode, the torsional degree of freedom can now be quantized. For a small rotation about the y direction, the Hamiltonian can be linearized and takes the form

$$H_{\text{meca}} = \frac{1}{2} I_y \omega_\phi^2 \hat{\phi}^2 + \frac{\hat{L}^2}{2 I_y}, \quad (7)$$

where ω_ϕ is the torsional frequency, I_y the moment of inertia and L the angular momentum. It can now be written in the form of a harmonic oscillator with the two variables \hat{L} and $\hat{\phi}$. In analogy with the canonical conjugate observable \hat{X} and \hat{P} of the center of mass mode, one can define annihilation and creation operators \hat{a} and \hat{a}^\dagger such that

$$\begin{aligned}\hat{\phi} &= \phi_0(\hat{a}^\dagger + \hat{a}), \quad \text{where } \phi_0 = \sqrt{\hbar/(2I_y\omega_\phi)}, \\ \hat{L} &= I_y\dot{\hat{\phi}} = iL_0(\hat{a}^\dagger - \hat{a}), \quad \text{where } L_0 = \sqrt{\hbar I_y\omega_\phi/2}.\end{aligned}\quad (8)$$

Because of its multivalued character, quantization of the canonical conjugate angle and orbital angular momenta has been a controversial debate [22]. Here, in the Paul trap, the angle is stabilized so that its value remains close to zero at all times, thus ensuring that the problem is analogous to the position and momentum degrees of freedom. A single quantum of motion will here have an angular extension ϕ_0 inversely proportional to the square root of the moment of inertia I_y .

A. Hamiltonian for torsional optomechanics

Having derived the values of the trapping frequency for the torsional mode, we now turn to the estimation of the coupling strength between the NV center spin and the torsional mode. The NV center has an inherent quantization axis given by the magnetic interaction between two electronic spins in the ground state. We take a NV center aligned along the rotating Z axis, which oscillates around the z axis as depicted in figure 1-a). In the presence of a homogeneous transverse magnetic field along x , if the nanodiamond rotates, the projection of the spin component along the magnetic field is modulated, thus providing a means to read-out and couple to the torsional mode. The Hamiltonian $\hat{H}_B = \hbar g_s \mu_B \vec{B} \cdot \hat{\vec{S}}$ describes the coupling of the spin to the transverse B field. We take \hat{S}_x and \hat{S}_z the spin operators along the X and Z rotating axis and assume the NV center to be located at the center of mass of the diamond. We have : so that

$$\hat{H}_B = \hbar \mu_B B \left(\sin \hat{\phi} \hat{S}_z + \cos \hat{\phi} \hat{S}_x \right). \quad (9)$$

Considering only first order terms in $\hat{\phi}$, the Hamiltonian becomes:

$$\hat{H}_B = \hbar g_s \mu_B B \phi_0 (\hat{a} + \hat{a}^\dagger) \hat{S}_z + \hbar g_s \mu_B B \hat{S}_x. \quad (10)$$

The total Hamiltonian of the system then writes :

$$\hat{H} = \hbar \omega_\phi \hat{a}^\dagger \hat{a} + \hat{H}_{\text{NV}} + \hbar \lambda_\phi (\hat{a} + \hat{a}^\dagger) \hat{S}_z, \quad (11)$$

where \hat{H}_{NV} is the Hamiltonian of the NV spin without the optomechanical coupling term and where the single quantum of motional shift is given by

$$\lambda_\phi = g_s \mu_B B \phi_0. \quad (12)$$

We have

$$\hat{H}_{\text{NV}} = D \hat{S}_z^2 + \hbar g_s \mu_B B \hat{S}_x + \hbar \Omega_R \hat{S}_y \cos(\omega t). \quad (13)$$

The first term $D \hat{S}_z^2$ describes spin-spin coupling between the two electron in the ground states and lifts the degeneracy between the three states of this spin 1 system. For the NV center, $D = 2.87$ GHz. The transverse constant magnetic field here mixes the ground and excited electronic states $|0\rangle$, $|\pm 1\rangle$ into mixed states $|g\rangle$, $|d\rangle$ and $|e\rangle$. The third term describes the coupling between the NV electronic spin and a microwave that is linearly polarised along the y axis, at a frequency ω and Rabi frequency Ω_R . In the absence of the microwave field, the eigenstates of \hat{H}_{NV} are $|d\rangle = (|-1\rangle - |1\rangle)/\sqrt{2}$, $|g\rangle = \cos \theta |0\rangle - \sin \theta |b\rangle$, $|e\rangle = \sin \theta |0\rangle + \cos \theta |b\rangle$ where $|b\rangle = (|-1\rangle + |1\rangle)/\sqrt{2}$, $\tan 2\theta = 2\gamma B/D$ and with energies $\omega_{e/g} = D \left(1 \pm \sqrt{1 + (2\gamma B/D)^2} \right)/2$, $\omega_d = D$.

In the basis of these vectors, we have :

$$\hat{S}_y = (\cos \theta |d\rangle \langle g| + \sin \theta |e\rangle \langle d| - h.c.) / i.$$

In our case, we consider $\omega \sim \omega_{dg} = \omega_d - \omega_g \neq \omega_{ed}$ so that the microwave only drives the transition between the $|g\rangle$ and $|d\rangle$ mixed states, as is depicted in Fig. 1-c).

In fig. 2-a) the energies of these states are plotted as a function of the magnetic field and the transition driven by the microwave is indicated for a specific magnetic field.

We now move in a frame at the microwave frequency. In this frame, \hat{H}_{NV} reads

$$\hat{H}_{\text{NV}} = \hbar/2 \begin{pmatrix} -\Delta & 0 & 0 \\ 0 & \Delta & 0 \\ 0 & 0 & \omega_{e'} \end{pmatrix} + \hbar/2i \begin{pmatrix} 0 & -\Omega_R & 0 \\ \Omega_R & 0 & 0 \\ 0 & 0 & 0 \end{pmatrix}, \quad (14)$$

where $\Delta = \omega - \omega_{dg}$, $\omega_{e'} = \omega_e - (\omega + \omega_g + \omega_d)/2$ and the energy origin has been set to $(\omega_g + \omega_d)/2$.

The new eigenstates of this hamiltonian are now $|e\rangle$ and $|+\rangle = i \sin \psi |g\rangle + \cos \psi |d\rangle$ and $|-\rangle = -i \cos \psi |g\rangle + \sin \psi |d\rangle$, where $\tan 2\psi = \Omega_R/\Delta$ and with $\omega_{+/-} = \pm \sqrt{\Delta^2 + \Omega_R^2}/2$. In the new eigenstate basis $|+\rangle$, $|-\rangle$, $|e\rangle$, the Hamiltonian can be approximated by a Rabi Hamiltonian :

$$\begin{aligned}\hat{H} &= \hbar \omega_\phi \hat{a}^\dagger \hat{a} + \hbar \omega_+ |+\rangle \langle +| + \hbar \omega_- |-\rangle \langle -| + \hbar \omega_{e'} |e\rangle \langle e| \\ &\quad + \hbar \tilde{\lambda}_\phi (\hat{a} + \hat{a}^\dagger) (|e\rangle \langle +| + h.c.),\end{aligned}\quad (15)$$

where $\tilde{\lambda}_\phi = \lambda_\phi \cos \theta \sin \psi$, which in turn can be reduced to a Jaynes-Cummings Hamiltonian under the condition that $\tilde{\lambda}_\phi \lesssim 10|\omega_e - \omega_+|$ and if we neglect the off-resonant terms [23]. Here, we set the microwave such that only the states $|+, N\rangle$ and $|e, M\rangle$ (with $M - N = \pm 1$, M and N being the phonon numbers) are resonant, *i.e.* $\omega_{e'} - \omega_+ = \omega_\phi$. In equation (15), the other terms $|+\rangle \langle -|$ and $|e\rangle \langle -|$ are neglected in the rotating wave approximation.

Fig. 2-b) depicts the $|+, N\rangle$ and $|e, M\rangle$ states in the resonant condition $\omega_{e'} - \omega_+ = \omega_\phi$: in the strong coupling regime, this Hamiltonian allows us to obtain a coherent exchange between torsional phonons and spin states at a rate $\lambda_\phi = \lambda_\phi \cos \theta \sin \psi$.

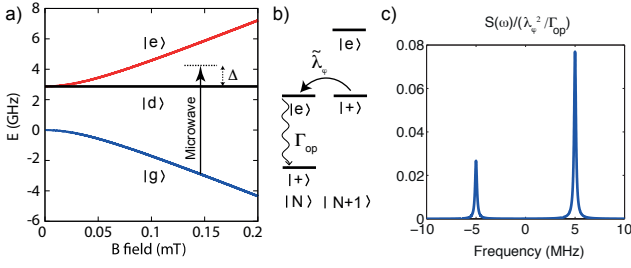


FIG. 2: (a) Energy of the spin eigenstates in presence of a transverse magnetic field. A microwave field is set close to resonance with ω_{gd} . (b) Optomechanical coupling between the dressed state $|+\rangle$ and $|e\rangle$ with phonon number N and $N+1$, under resonant condition. The wavy arrow indicates the optical pumping process that allows the cooling mechanism. Although not represented here, this process works both ways and also affects the $|-\rangle$ state. (c) Spectrum obtained for emission ($\omega < 0$) or absorption ($\omega > 0$) of phonons under resonant conditions $\omega_e - \omega_+ = \omega_\phi$. The parameters are : $\omega_\phi = 5$ MHz, $B = 0.07$ T, $\Omega = 1$ GHz, $\Delta = 800$ MHz, $\Gamma_{op} = 100$ kHz, $\alpha = 1$.

B. Cooling mechanism

A cooling scheme can be set up similarly to [6] by adding an optical field to excite the electronic states. Optical pumping polarizes the spin state to the $|0\rangle$ state through non-radiative decay via a metastable state [24]. Taking into account this dissipative process and the unitary evolution of the system, we obtain unbalanced populations of the $|+\rangle$ and $|e\rangle$ states, enabling continuous cooling through coupling with the phonon. Contrary to [6], neither $|+\rangle$ nor $|e\rangle$ is orthogonal to $|0\rangle$: the depopulation -and cooling- therefore only occur if we ensure the probabilities $\langle 0|e\rangle$ and $\langle 0|+\rangle$ to be sufficiently unbalanced. This can be tuned using the magnetic field, the microwave detuning and Rabi frequency. Moreover, the optical polarization is not perfect: at room temperature, a fraction $\alpha \sim 1$ of the optically excited states decays to the same spin states, reducing the efficiency of the cooling process.

To study how the cooling efficiency varies with the B field and microwave parameters, we look for the phonon mean occupation number. First, we separate the spin dynamics [6, 25] by considering it to be much faster than the phonon one ($\omega_r, \Gamma_{op} \gg \tilde{\lambda}_\phi$). The master equation for the spin degree of freedom therefore becomes :

$$\dot{\hat{\rho}} = i[\hat{\rho}, \hat{H}] / \hbar + \Gamma_{op} \sum_{i=\pm 1} (D[|0\rangle\langle i|] + \alpha D[|i\rangle\langle i|]), \quad (16)$$

where Γ_{op} is the optical pumping rate and $D[\hat{c}] = \hat{c}\hat{\rho}\hat{c}^\dagger - (\hat{c}^\dagger\hat{c}\hat{\rho} + \hat{\rho}\hat{c}^\dagger\hat{c})/2$. The Lindblad superoperator $D[\hat{c}]$ is here used to describe the dissipative decay to the $|0\rangle$ state with a rate Γ_{op} or to the same spin state with a rate $\alpha\Gamma_{op}$. The effect of the spin lifetime and decoherence are neglected, since the considered rates

are expected to be much slower than the spin dynamics.

The total cooling rate is $W = W_{op} + W_{gas}$ where W_{gas} is the heating rate due to residual gas and $W_{op} = S(\omega_\phi) - S(-\omega_\phi)$ is the optical cooling rate determined by the fluctuation spectrum [6] :

$$S(\omega) = 2\lambda_\phi^2 \int_0^\infty d\tau \langle \hat{S}_z(\tau) \hat{S}_z(0) \rangle e^{i\omega\tau}. \quad (17)$$

For a given set of parameters, we use the master equation and the quantum regression theorem to obtain the fluctuation spectrum and in turn the cooling rate. This was done numerically using Matlab. In fig. 2-c) the fluctuation spectrum is plotted under resonant conditions for the $|e\rangle$ and $|+\rangle$ states and with a Rabi frequency larger than the microwave detuning. With such parameters, the red sideband is higher than the blue sideband showing continuous cooling (*i.e.* $W > 0$).

Fig. 3 shows the dimensionless value W_{op}/R_B , where $R_B = (g_s \mu_B B_0 \phi_0)^2 / \Gamma_{op}$, and $B_0 = 0.07$ T when varying the B-field and the microwave detuning (ψ parameter). A high cooling rate can be achieved for $\phi/\pi = 0.15$ and under magnetic fields above 100 mT. There is a practical limitation to accessing the area of this map however : as the magnetic field is increased, the resonance condition ($\omega_e - \omega_+ = \pm \omega_\phi$) requires a large splitting $\sqrt{\Delta^2 + \Omega_R^2}$ of the $|+\rangle$ and $|-\rangle$ states. Since it is technically challenging to increase Ω_R above the GHz range [26], one will have to increase Δ therefore limiting oneself to the lower ψ .

The ψ parameter that allows resonant conditions for a Rabi frequency of 1 GHz is plotted in Figure 3 as a function of the magnetic field. This figure also shows that for such a Rabi frequency the cooling rate reaches an optimum for a moderate magnetic field of about 70 mT, as shown by the dashed lines.

C. Final phonon occupation number

The final phonon occupation number under continuous cooling is given by :

$$\langle n \rangle_0 = \frac{A_{op}^+ + W_{gas}}{W_{op}}, \quad (18)$$

[6, 25], with $A_{op}^+ = S(-\omega_\phi)$ the optical heating rate. In [27], W_{gas} was evaluated for the center of mass mode of nanospheres as a function of the pressure. Here we work under the assumption that this heating rate is in the same range for the torsional modes, although further investigations are needed to determine how correct is this assumption. We consider a diamond sphere with a 35 nm radius under a vacuum pressure of 10^{-8} mbar. Under a magnetic field $B_0 = 70$ mT and with a Rabi frequency of 1 GHz, the final phonon number is found to be $\langle n \rangle_0 = 0.51$, already close to the ground state.

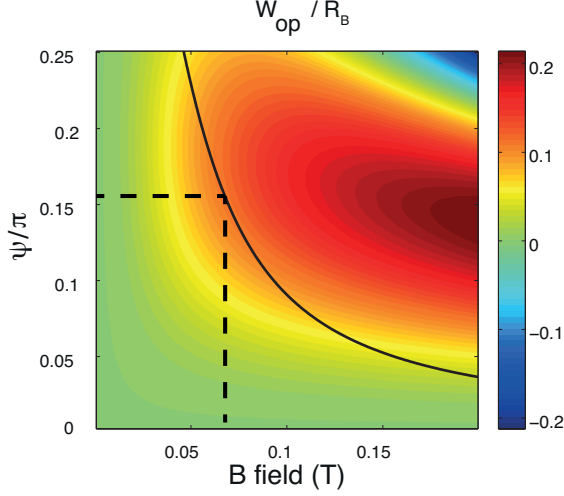


FIG. 3: Normalized cooling rate as a function of the B -field and Ψ/π . The black line is the ψ parameter under resonant conditions and with $\Omega_R = 1$ GHz as a function of the B -field. $\Gamma_{\text{op}}=100$ kHz, $\omega_\phi=5$ MHz and $\alpha=1$.

A “pulsed pumping strategy” as discussed in [6] would allow one to go beyond this number. Another option is to tune the B -field again. Provided W_{gas} is much smaller than W_{op} , the cooling rate can be reduced and $\langle n \rangle_0$ increased. This can be seen by the fact that the λ_ϕ dependency cancels in $\langle n \rangle_0$. Cooling to the ground state can be obtained for lower magnetic fields, and with a lower Rabi frequency. For a Rabi frequency of 20 MHz at a magnetic field of 16 mT we actually find a final phonon number $\langle n \rangle_0 = 0.036$, very close to the ground state. Let us note that some limitations discussed in sec. IV are not taken into account and would then require a higher cooling rate.

Achieving ground state cooling is an important preliminary step towards preparing arbitrary phonon Fock states [28]. This is however possible only if the strong coupling regime is reached.

III. STRONG COUPLING REGIME

A. Size and geometry

Let us now describe the conditions to be in the strong coupling regime. The crucial parameters to attain the strong coupling regime can be extracted from the formulas $\phi_0 = \sqrt{\hbar/2I_y\omega_\phi}$ and $\omega_\phi \sim \frac{QS_\mu}{I_\mu} \frac{V_{ac}}{z_0^2} \frac{1}{\Omega}$. The angular frequency ω_ϕ must be higher than the width of the electron spin resonance to achieve sideband cooling and coherent manipulation. Also, ϕ_0 must be high enough in order for the phonon-photon coupling rate $\tilde{\lambda}_\phi = \lambda_\phi \cos\theta \cos\psi$ to be higher than all decoherence rates. Both ω_ϕ and ϕ_0 depend on parameters that are

both intrinsic and extrinsic to the diamond. Because of the $\cos\theta$ term in $\tilde{\lambda}_\phi$, the B -field cannot be increased above ~ 70 mT. The other extrinsic parameters such as the Paul trap V/z^2 and Ω can be increased to tune the frequency ω_ϕ . Technical limitations will however set an upper bound: the Paul trap should not be smaller than a few tens of microns and reaching a voltage higher than a few thousands volts at high frequencies will be challenging. The intrinsic parameters of the diamond particle are then the only parameters we can tune.

The frequency that must be attained is determined by both the quality of the diamond and the distance of the NV center from the surface, hence by the diameter d of the considered diamond. However, one can see that decreasing the size of the diamond can considerably increase the trapping frequency, since the $\frac{QS_\mu}{I_\mu} = \frac{\sigma SS_\mu}{I_\mu}$ scales as $\frac{1}{d}$, provided the charge density on the diamond surface is independent on d . Then, the factor $\frac{QS_\mu}{I_\mu}$ depends strongly on the geometry. To obtain a high ϕ_0 , one also requires to have a low inertia momentum. This also points towards using small particles and highlights the relevance of the geometry.

In short, micron-size diamonds do not lend themselves easily to ground state cooling since they are heavier, but they will retain the photophysical properties of bulk diamonds. Conversely, nanodiamonds have shorter coherence time than in the bulk but faster cooling can be reached. By tuning the aspect ratio of particles one can however find a compromise.

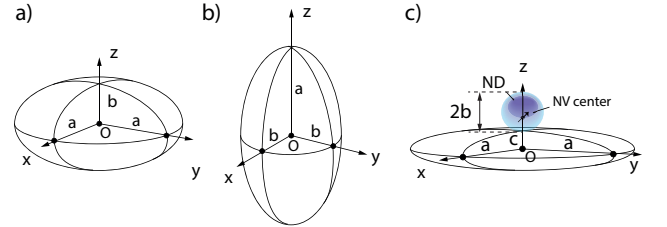


FIG. 4: Shapes of the proposed asymmetric particles: a) oblate ellipsoid, b) prolate ellipsoid and c) composite particle formed by a diamond sphere deposited on a thin disk, approximated by an oblate ellipsoid.

Three geometries have been envisioned and are depicted in figure 4: oblate and prolate ellipsoids, and composite particles formed by a diamond sphere deposited on a thin disk. This last shape enables choosing any material for the disk and thus optimize the charge to mass ratio and trapping frequency independent on the diamond. For all shapes, the b and a parameters always correspond to the minimum, resp. maximum, particle radius. In table I, the trapping frequencies and moment of inertia are calculated for these shapes. They are normalized with respect to the trapping frequencies (ω_0) and moment of inertia (I_0) of a sphere with the same radius b . It is indeed important to compare particles with the same minimum radius to ensure that the NV prop-

particle type	c/b	ω_{com}/ω_0	ω_ϕ/ω_0	ω_ϕ/ω_{com}	I_y/I_0
sphere	-	1	0	0	1
oblate ellipsoid	-	0.64	1.8	2.9	23
prolate ellipsoid	-	0.83	2.3	2.8	9
composite	0.125	2.8	19	5.3	2.4
composite	0.0625	3.3	27.6	6.3	1.2

TABLE I: Comparison of the mechanical parameters of different particles shapes, as shown in fig. 4 for the same b , for the same aspect ratio $a/b = 2.5$ and identical surface charge density. ω_0 and I_0 are the secular frequency of the center of mass and the moment of inertia of a sphere with radius b respectively. For each considered particles, ω_{com} and ω_ϕ are the secular frequencies of the center of mass and the torsional modes respectively, I_y is the moment of inertia.

erties (which depend crucially on their distance from the surface) are the same. The torsional frequency is also compared to the center of mass mode ω_{com} , for the same b and for an aspect ratio $a/b = 2.5$. The trapping frequencies were calculated by integrating the torque over the surface of the ellipsoids, considering a homogeneous surface charge. Looking at table I, one sees that particles with a higher asymmetry and spatial extent experience a higher torsional trapping frequency. They however also have a greater moment of inertia, which reduce the coupling λ_ϕ . To both increase the trapping frequency and reduce the inertia momentum without reducing the size of the particle, the proposed composite particle comprising a spherical diamond of size b within or deposited on a thinner disk of silica allows to considerably increase the confinement of the particle with a moment of inertia much smaller than with simpler shapes, as can be seen in table I.

B. Experimental implementation

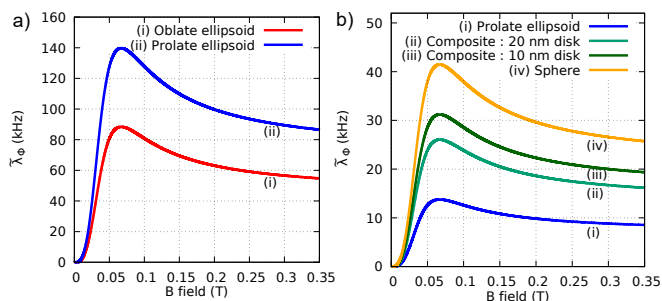


FIG. 5: a) Coupling rate $\tilde{\lambda}_\phi$ for nanodiamonds of different shapes as described in fig. 4 with a) $b = 20$ nm and with a torsional confinement $\omega_\phi = 5$ MHz and b) with $b = 80$ nm and a torsional confinement $\omega_\phi = 0.5$ MHz. The aspect ratio of the proposed particles, as described in fig. 4, with $a/b = 2.5$ for all particles and $c/b = 0.125, 0.0625$ for the composite 20 nm and 10 nm disks respectively.

Optical tweezers already showed not only rotational stability [15] and control [29], but also torsional vibration frequencies up to several MHz [30]. The main challenge for an implementation of the proposed cooling scheme with a Paul trap is to attain such high frequencies. As stated above reducing the size of the particle to obtain a better charge to mass ratio and engineer its shape would increase the torsional confinement.

In figure 5, the coupling rate $\tilde{\lambda}_\phi$ is plotted as a function of the magnetic field. Fig. 5-a) shows the coupling rate for particles with radius $b = 20$ nm : a maximum is reached in the range of 100 kHz with a B field $B_0 = 70$ mT. In fig. 5-b) the considered particles are chosen to have a radius $b = 80$ nm. The coupling rate for a prolate ellipsoid is much smaller, barely exceeding 10 kHz, it can however be increased by using the proposed composite particle : it will then depend on how thin can the disk of the composite particle be. The coupling rate with a zero-mass disk (*i.e.* for a sphere) is plotted as a limit for such particles.

The so-called strong coupling regime is reached for $T_1, T_2 \gg 1/\tilde{\lambda}_\phi$, where $T_2^{-1} = (2T_1)^{-1} + (T_2^*)^{-1}$, and $(T_2^*)^{-1}$ is the inhomogeneous decoherence rate due to the coupling to a nuclear spin bath. For very shallow (5 nm deep) NV centers, T_1 ranges from several hundreds of microseconds to milliseconds [31], the main constraint for reaching the strong coupling regime is the T_2^* time. Studies using dynamical decoupling sequences show that NV center within 50 nm diameter nanodiamonds synthesised through reactive ion etching (RIE) [32] of CVD-grown diamonds should reach T_2 times of up to 200 μs using ^{12}C isotopically engineered diamond [33, 34]. It was indeed shown that the main source of degradation of the T_2 is the ^{13}C nuclear spin bath. For particles with a 20 nm minimum bulk radius, a $T_2 \sim 100 \mu s$ would already allow entering the strong coupling regime. For 80 nm particles diameters, T_2 is expected to be closer to bulk values, and can attain $T_2 \sim 1.8$ ms [33]. Here $T_2 \gtrsim 500 \mu s$ would be sufficient to reach the strong coupling regime.

We note that, even though advances have been made in engineering the shape of nanodiamonds, the proposed ellipsoid particles are an approximation of the particle shapes of [32, 35, 36]. RIE [32, 37] is however quite adapted for torsional optomechanics, since diamonds can be engineered to form nano-pillars that are close to prolate ellipsoid particles and can thus reach high torsional trapping frequencies.

IV. LIMITATIONS

A. Internal temperature

The most direct problem that one may foresee with room temperature diamonds is the potential coupling between internal (phonon) and external degrees of freedom. Indeed, the zero-point motion of nanodiamonds is a few picometers, on the order of the atomic displacement in-

duced by phonons. The influence of the coupling between vibrational degrees of freedom and external ones was studied in detail in [38]. It is argued that the large difference in frequencies between the center of mass modes (MHz range) and the internal phonons modes (THz) enables adiabatic elimination of the vibrational energy levels, yielding the result that the only effect is a second order shift of the trapping frequency. This effect can thus be neglected here too.

B. Laser heating

A levitating system with charged particles constitutes an extreme example of environmental isolation because the center of mass motion is naturally decoupled from the internal degrees of freedom in addition to being mechanically isolated by levitation. In this case, the decoherence and cooling rates are fundamentally limited by the momentum recoil of the scattered photons used for polarizing the NV center's spin. For instance, the 532nm laser that will be used for cooling may induce heating of the torsional mode and also heat the diamond itself thereby affecting the photo-physics of the NV centers. To ensure that the green laser does not heat up the cooled mode, a green laser direction that is along the rotation axis of that torsional mode can be chosen in order to minimize the random recoil kicks due to the laser in that mode.

Another important effect is the heating of the diamond itself due to the laser, which can have detrimental consequences on the photophysics of NV centers. A pulsed scheme and high purity diamonds can however be used

to go beyond 10^{-2} mbars of vacuum pressure observed in [39]. It is however difficult to give a precise estimate of the total laser induced heating rate of the diamond at low vacuum pressures, which depends critically on the nanodiamond size, shape and purity [16, 40].

Conclusion

We have shown how one can benefit from the original spin properties of the NV center to obtain a torsional opto-mechanical coupling using a nanodiamond levitating in a Paul trap. Working with the torsional degree of freedom instead of the center of mass allows not only to circumvent the necessity to have a strong magnetic gradient [6, 9], but also to increase the oscillators frequency. We show that continuous cooling of the torsional mode with phonon numbers well below unity is achievable. We finally discuss how this scheme enables entering the strong coupling regime for different particle sizes and shapes.

Note : During the preparation of this manuscript, related work by Zhang-qi Yin and coworkers was presented in [41].

Acknowledgements

We would like to acknowledge fruitful discussions with Peter Rabl. This research has been partially funded by the French National Research Agency (ANR) through the project SMEQUI.

-
- [1] M. Aspelmeyer, T. J. Kippenberg, and F. Marquardt, *Rev. Mod. Phys.* **86**, 1391 (2014).
 - [2] C. Reinhardt, T. Müller, A. Bourassa, and J. C. Sankey, *Physical Review X* **6**, 021001 (2016).
 - [3] R. A. Norte, J. P. Moura, and S. Gröblacher, *Physical review letters* **116**, 147202 (2016).
 - [4] Y. Tsaturyan, A. Barg, E. S. Polzik, and A. Schliesser, *arXiv preprint arXiv:1608.00937* (2016).
 - [5] P. Treutlein, D. Hunger, S. Camerer, T. W. Hänsch, and J. Reichel, *Phys. Rev. Lett.* **99**, 140403 (2007).
 - [6] P. Rabl, P. Cappellaro, M. V. G. Dutt, L. Jiang, J. R. Maze, and M. D. Lukin, *Phys. Rev. B* **79**, 041302 (2009).
 - [7] O. Arcizet, V. Jacques, A. Siria, P. Poncharal, P. Vincent, and S. Seidelin, *Nat Phys* **7**, 879 (2011).
 - [8] S. Kolkowitz, A. C. Bleszynski Jayich, Q. P. Unterreithmeier, S. D. Bennett, P. Rabl, J. G. E. Harris, and M. D. Lukin, *Science* **335**, 1603 (2012).
 - [9] Z. Yin, N. Zhao, and T. Li, *Science China Physics, Mechanics & Astronomy* **58**, 1 (2015).
 - [10] D. E. Chang, C. A. Regal, S. B. Papp, D. J. Wilson, J. Ye, O. Painter, H. J. Kimble, and P. Zoller, *Proceedings of the National Academy of Sciences* **107**, 1005 (2010).
 - [11] M. Scala, M. S. Kim, G. W. Morley, P. F. Barker, and S. Bose, *Phys. Rev. Lett.* **111**, 180403 (2013).
 - [12] Z.-q. Yin, T. Li, X. Zhang, and L. M. Duan, *Phys. Rev. A* **88**, 033614 (2013).
 - [13] L. P. Neukirch, J. Gieseler, R. Quidant, L. Novotny, and A. Nick Vamivakas, *Optics Letters* **38**, 2976 (2013).
 - [14] V. R. Horowitz, B. J. Alemán, D. J. Christle, A. N. Cleland, and D. D. Awschalom, *Proceedings of the National Academy of Sciences* **109**, 13493 (2012).
 - [15] M. Geiselmann, M. L. Juan, J. Renger, J. M. Say, L. J. Brown, F. J. G. de Abajo, F. Koppens, and R. Quidant, *Nat Nano* **8**, 175 (2013).
 - [16] A. C. Frangskou, A. T. M. A. Rahman, L. Gines, S. Mandal, O. A. Williams, P. F. Barker, and G. W. Morley, *ArXiv e-prints* (2016), 1608.04724.
 - [17] A. T. M. A. Rahman, A. C. Frangskou, M. S. Kim, S. Bose, G. W. Morley, and P. F. Barker, *Scientific Reports* **6**, 21633 EP (2016).
 - [18] T. M. Hoang, J. Ahn, J. Bang, and T. Li, *Nature Communications* **7**, 12250 EP (2016).
 - [19] A. Gruber, A. Drbenstedt, C. Tietz, L. Fleury, J. Wrachtrup, and C. v. Borczyskowski, *Science* **276**, 1212 (1997).
 - [20] A. Kuhlicke, A. W. Schell, J. Zoll, and O. Benson, *Applied Physics Letters* **105** (2014).
 - [21] T. Delord, L. Nicolas, L. Schwab, and G. Hétet, *arXiv*

- preprint arXiv:1605.02953 (2016).
- [22] H. A. Kastrup, Phys. Rev. A **73**, 052104 (2006).
 - [23] D. Braak, in *Applications+ Practical Conceptualization+ Mathematics= fruitful Innovation* (Springer, 2016), pp. 75–92.
 - [24] L. Robledo, H. Bernien, T. van der Sar, and R. Hanson, New Journal of Physics **13**, 025013 (2011).
 - [25] J. I. Cirac, R. Blatt, P. Zoller, and W. Phillips, Physical Review A **46**, 2668 (1992).
 - [26] G. Fuchs, V. Dobrovitski, D. Toyli, F. Heremans, and D. Awschalom, Science **326**, 1520 (2009).
 - [27] O. Romero-Isart, M. L. Juan, R. Quidant, and J. I. Cirac, New Journal of Physics **12**, 033015 (2010).
 - [28] C. Law and J. Eberly, Physical review letters **76**, 1055 (1996).
 - [29] S. Kuhn, A. Kosloff, B. A. Stickler, F. Patolsky, K. Hornberger, M. Arndt, and J. Millen, arXiv preprint arXiv:1608.07315 (2016).
 - [30] T. M. Hoang, Y. Ma, J. Ahn, J. Bang, F. Robicheaux, Z.-Q. Yin, and T. Li, Phys. Rev. Lett. **117**, 123604 (2016).
 - [31] T. Rosskopf, A. Dussaux, K. Ohashi, M. Loretz, R. Schirhagl, H. Watanabe, S. Shikata, K. M. Itoh, and C. Degen, Physical review letters **112**, 147602 (2014).
 - [32] M. E. Trusheim, L. Li, A. Laraoui, E. H. Chen, H. Bakhru, T. Schrder, O. Gaathon, C. A. Meriles, and D. Englund, Nano letters **14**, 32 (2013).
 - [33] G. Balasubramanian, P. Neumann, D. Twitchen, M. Markham, R. Kolesov, N. Mizuochi, J. Isoya, J. Achard, J. Beck, J. Tissler, et al., Nature materials **8**, 383 (2009).
 - [34] J. Maze, J. Taylor, and M. Lukin, Physical Review B **78**, 094303 (2008).
 - [35] P. Appel, E. Neu, M. Ganzhorn, A. Barfuss, M. Batzer, M. Gratz, A. Tschöpe, and P. Maletinsky, Review of Scientific Instruments **87**, 063703 (2016).
 - [36] P. Andrich, B. J. Alemn, J. C. Lee, K. Ohno, C. F. de las Casas, F. J. Heremans, E. L. Hu, and D. D. Awschalom, Nano letters **14**, 4959 (2014).
 - [37] Applied Physics Letters **104**, 153108 (2014).
 - [38] O. Romero-Isart, A. C. Pflanzner, M. L. Juan, R. Quidant, N. Kiesel, M. Aspelmeyer, and J. I. Cirac, Phys. Rev. A **83**, 013803 (2011).
 - [39] T. Delord, L. Nicolas, M. Bodini, and G. Hétet, arXiv preprint arXiv:1701.06407 (2017).
 - [40] C. Zhong and F. Robicheaux, arXiv preprint arXiv:1701.04477 (2017).
 - [41] Y. Ma, T. M. Hoang, M. Gong, T. Li, and Z.-q. Yin, arXiv preprint arXiv:1611.05599 (2016).